

- not the differentially methylated DNA regions or antisense transcripts, marks the imprinting status of *IGF2R* in human and mouse. *Hum. Mol. Genet.* 13:2233-2245.
36. Wang, J., J. Mager, Y. Chen, E. Schneider, J. C. Cross, A. Nagy, and T. Magnuson. 2001. Imprinted X inactivation maintained by a mouse Polycomb group gene. *Nat. Genet.* 28:371-375.
  37. Wang, Y., K. Joh, S. Masuko, H. Yatsuki, H. Soejima, A. Nabetani, C. V. Beechey, S. Okinami, and T. Mukai. 2004. The mouse *Murr1* gene is imprinted in the adult brain, presumably due to transcriptional interference by the antisense-oriented *U2af1-rs1* gene. *Mol. Cell. Biol.* 124:270-279.
  38. Yamasaki, K., K. Joh, T. Ohta, H. Masuzaki, T. Ishimaru, T. Mukai, N. Niikawa, M. Ogawa, J. Wagstaff, and T. Kishino. 2003. Neurons but not glial cells show reciprocal imprinting of sense and antisense transcripts of *Ube3a*. *Hum. Mol. Genet.* 12:837-847.
  39. Yamasaki, Y., T. Kayashima, H. Soejima, A. Kinoshita, K. Yoshiura, N. Matsumoto, T. Ohta, T. Urano, H. Masuzaki, T. Ishimaru, T. Mukai, N. Niikawa, and T. Kishino. 2005. Neuron-specific relaxation of *Igf2r* imprinting is associated with neuron-specific histone modifications and lack of its antisense transcript *Air*. *Hum. Mol. Genet.* 14:2511-2520.
  40. Yang, Y., T. Li, T. H. Vu, G. A. Ulaner, J. F. Hu, and A. R. Hoffman. 2003. The histone code regulating expression of the imprinted mouse *Igf2r* gene. *Endocrinology* 144:5658-5670.

## Paroxysmal kinesigenic choreoathetosis (PKC): confirmation of linkage to 16p11-q21, but unsuccessful detection of mutations among 157 genes at the PKC-critical region in seven PKC families

Taeko Kikuchi · Masayo Nomura · Hiroaki Tomita · Naoki Harada · Kazuaki Kanai · Tohru Konishi · Ayako Yasuda · Masato Matsuura · Nobumasa Kato · Koh-ichiro Yoshiura · Norio Niikawa

Received: 22 November 2006 / Accepted: 13 January 2007 / Published online: 14 February 2007  
© The Japan Society of Human Genetics and Springer 2007

**Abstract** Paroxysmal kinesigenic choreoathetosis (PKC) is a paroxysmal movement disorder of unknown cause. Although the PKC-critical region (PKCCR) has been assigned to the pericentromeric region of chromosome 16 by several studies of families from various ethnic backgrounds, the causative gene has not yet been identified. In the present study, we performed linkage and haplotype analysis in four new families with PKC, as well as an intensive polymerase chain reaction (PCR) based mutation analysis in seven families for a total of 1,563 exons from 157 genes mapped around the PKCCR. Consequently, the linkage/haplotype analysis revealed that PKC was assigned to a 24-cM segment between *D16S3131* and *D16S408*, the result confirming the previously defined PKCCR, but being unable to narrow it down. Although the

mutation analysis of the 157 genes was unsuccessful at identifying any mutations that were shared by patients from the seven families, two nonsynonymous substitutions, i.e., 6186C>A in exon 3 of *SCNN1G* and 45842A>G in exon 29 of *ITGAL*, which were segregated with the disease in Families C and F, respectively, were not observed in more than 400 normal controls. Thus, one of the two genes, *SCNN1G* and *ITGAL*, could be causative for PKC, but we were not able to find any other mutations that explain the PKC phenotype.

**Keywords** Paroxysmal kinesigenic choreoathetosis (PKC) · PKC-critical region · Linkage analysis · Mutation analysis · *SCNN1G* · *ITGAL*

T. Kikuchi · M. Nomura · N. Harada · K. Yoshiura (✉) · N. Niikawa  
Department of Human Genetics, Nagasaki University  
Graduate School of Biomedical Sciences, Sakamoto 1-12-4,  
Nagasaki 852-8523, Japan  
e-mail: kyoshi@nagasaki-u.ac.jp

T. Kikuchi  
Department of Psychiatry, Nagasaki University Graduate  
School of Biomedical Sciences, Nagasaki, Japan

H. Tomita  
Department of Psychobiology, Graduate School  
of Medicine, Tohoku University, Sendai, Japan

N. Harada  
Kyushu Medical Science, Nagasaki, Japan

K. Kanai  
Department of Neurology, Chiba University School  
of Medicine, Chiba, Japan

T. Konishi  
Division of Pediatrics, Nagaoka Ryoikuen, Nagaoka, Japan

A. Yasuda  
Department of Pediatrics, Japanese Red Cross Nagoya First  
Hospital, Nagoya, Japan

M. Matsuura  
Section of Biofunctional Informatics, Graduate School  
of Allied Health Sciences, Tokyo Medical and Dental  
University, Tokyo, Japan

N. Kato  
Department of Psychiatry, Faculty of Medicine,  
University of Tokyo, Tokyo, Japan

T. Kikuchi · M. Nomura · N. Harada · K. Yoshiura ·  
N. Niikawa  
Solution Oriented Research of Science and Technology  
(SORST), Japan Science and Technology Agency (JST),  
Kawaguchi, Japan

**Introduction**

Paroxysmal kinesigenic choreoathetosis (PKC; MIM 128200) is a paroxysmal movement disorder characterized by recurrent and brief attacks of unilateral or bilateral involuntary movements, including dystonic posturing, chorea, athetosis, and ballism, which are precipitated by the sudden onset of movements (Kato et al. 2006). The attacks can last as long as a few seconds to a few minutes, occur up to 100 times daily, but usually manifest in childhood or early adolescents, and commonly decrease with age. There is no loss of consciousness during these attacks. The attacks are responsive to anticonvulsants such as carbamazepine or phenytoin. Electroencephalogram (EEG) analysis demonstrates normal or nonspecific abnormalities. Neuroimaging and neuropathological studies resulted in unremarkable findings (Sadamatsu et al. 1999; Nagamitsu et al. 1999). The etiology and pathophysiology of PKC still remain unclear. Some neurologists consider PKC as a form of reflex epilepsy, whereas others believe that basal ganglia dysfunction may play a role in its cause (Kato et al. 2006). Most (40–70%) were familial cases in which PKC was transmitted in an autosomal dominant mode of inheritance with incomplete penetrance (Tomita et al. 1999; Valente et al. 2000). Males are affected more often than females, with an estimated ratio of 3–4:1 (Bhatia 1999).

We previously performed a genome-wide linkage and haplotype analysis in eight Japanese families with PKC and defined the disease locus within a 12.4-cM region between *D16S3093* and *D16S416* at 16p11.2-q12.1 (Tomita et al. 1999). This PKC-critical region (PKCCR) was confirmed by others (Bennett et al. 2000; Swoboda et al. 2000; Valente et al. 2000; Cuenca-Leon et al. 2002). In addition, mapped regions for other conditions probably allelic to PKC, such as infantile convulsions and paroxysmal choreoathetosis (ICCA; MIM 602066) and benign familial infantile convulsions (BFIC2; MIM 605751), shared with that for PKC (Lee et al. 1998; Hattori et al. 2000; Swoboda

et al. 2000; Caraballo et al. 2001; Weber et al. 2004). Nevertheless, mutations in any genes within the PKCCR have remained uncovered.

Here, we describe the results of the mutation analyses of seven PKC families for a total of 157 genes located at or around the PKCCR, together with linkage/haplotype analysis of four newly identified families.

**Materials and methods**

**Subjects**

The subjects studied included seven families (Families A–G) with PKC. Two of them (Families F and G) corresponded respectively to Families 1 and 3 in our previous report (Tomita et al. 1999), and five other families (Families A–E, Fig. 1) were those which were newly collected. A total of 21 members, including 16 PKC patients from four of the five families (Families A–D), underwent a linkage and haplotype analysis. In addition, one of each affected individual (we further call them representative patients) chosen from all seven families was subjected to mutation analysis. Blood samples were collected from all participants after obtaining written informed consent, and the study protocol was approved by the Committee for Ethical Issues on Human Genome and Gene Analysis at Nagasaki University.

**Genotyping and linkage analysis**

Genomic DNA was isolated from the blood lysate of the 21 participants by phenol-chloroform extraction, followed by ethanol precipitation. To try to narrow down the PKCCR, we performed genotyping and haplotype analysis in the four newly collected PKC families, using 13 microsatellite markers (Table 1) located to a 36-cM region at 16p12-q21 to which PKC has been shown to be linked, as well as using three

**Fig. 1** Pedigree of the five families (Families A–E) with paroxysmal kinesigenic choreoathetosis (PKC). The closed squares and circles denote individuals affected with PKC. Although not shown here, Families F and G correspond to Families 1 and 3 reported previously (Tomita et al. 1999)

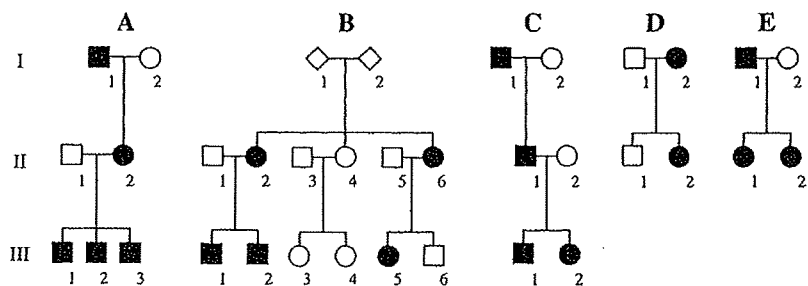


**Table 1** Primer sequences of the 12 microsatellite markers used for genotyping and linkage analysis

Markers	Forward primer (5'–3')	Reverse primer (5'–3')
D16S403	CAAGACTAACGCTGATGGCT	GACAGTGAGGTGGGAATCAAA
D16S417	CTGTCCAACATGCAGCC	TGAAGTCAATCCCCTTGAA
D16S3131	CTGCTTCCATCTTGCC	CTAGCCCCCAAATGTG
D16S3093	CAAGGGCAAACTCCAT	CCAAAAGGTTGATTCTCTG
AC007353-M1	GCTTAACTACATTTTATTCAAGGTTG	TCTGTGGTAGAGAGGGCAAAGA
AC092368-M1	GTTTACCAGCCATTTTAAATCAACA	TGAATAAGTGTGTCTTTCAACAAAATT
AC092721-M3	GCCCTGTAATATAATTTGAAGTTG	GGGTTCAAGTGATTCTCCTG
D16S3136	CTCACCTATTGCCCTCAAGAA	CAGAATCTTATGCCATTATT
D16S416	CATAGGACCCTCAGATGTATA	CTGCCTATGGCTAAGAGGACA
D16S408	TGTAACCTTGTGTGCATCCT	CACTCTTATCCCAGGAACCC
D16S514	CAATTCTTGATGCTACCAT	CTTGTCTAGTGGCTGGAATA
D16S3143	GCTACTGAGGAAACCTTATCC	GGCCATTACAGGAAGTGC

Primers of D16S3068 were purchased from the ABI PRISM Linkage Mapping Sets LMS (Applied Biosystems, Foster City, CA)

additional markers (AC007353-M1, AC092368-M1, and AC092721-M3) that were designed by us according to the human genome sequence (<http://genome.cse.ucsc.edu/>). Sample DNA was polymerase chain reaction (PCR) amplified for each marker locus with fluorescence-labeled primers. PCR was performed on DNA Thermal Cycler Model 9700 (Applied Biosystems, Foster City, CA) in a 10- $\mu$ l reaction mixture containing 1 $\times$ PCR buffer (Takara Bio, Otsu, Japan), 200  $\mu$ M each of dNTP, 0.5  $\mu$ M each of primer, 10 ng DNA, and 0.25 units ExTaq DNA polymerase HS-version (Takara Bio, Otsu, Japan) under the conditions of denaturation at 94°C for 2 min, 35 cycles of 94°C for 30 s, 58°C for 30 s, and 72°C for 1 min, and final extension at 72°C for 7 min. PCR products were run on an auto-sequencer Model 3100 (Applied Biosystems, Foster City, CA). Allele sizes were analyzed by GeneScan and Genotyper software (Applied Biosystems, Foster City, CA) to determine the genotypes.

#### Mutation analysis

We performed PCR-based mutation analysis of the seven representative patients with typical features of PKC. Sequences examined for mutations among the seven patients included those of 1,371 coding exons, excluding the 3'-UTR and 5'-UTR in 117 genes, located at the PKCCR between *D16S3093* and *D16S416* (Table 1). The analysis in five families (Families A and C–F) was expanded to an additional 192 exons of 40 other genes, whereas because of depletion of genomic DNA, an expanded analysis was not done in the remaining two families. Thus, a total of 1,563 exons in 157 genes were analyzed for mutation (primer sequences are available on request).

#### Real-time quantitative PCR

We performed real-time quantitative PCR in six representative patients from Families A and C–G. Six pairs of primers and TaqMan probes were designed for exons 1, 6, and 13 of *SCNN1G*, and for exons 1, 16, and 30 of *ITGAL*. PCR was carried out in a 10- $\mu$ l reaction mixture containing 5  $\mu$ l of 2 $\times$ TaqMan Universal PCR Master mix (Applied Biosystems, Foster City, CA), 0.4  $\mu$ M each of primer, a 0.2- $\mu$ M probe, and 10 ng DNA under the conditions of 2 min at 50°C, 10 min at 95°C, 40 cycles of 15 s at 95°C, and 1 min at 60°C, with a 7900HT Sequence Detection System (Applied Biosystems, Foster City, CA).

#### Results

The haplotype analysis showed that all affected individuals in the four new families share an allele at each locus examined between *D16S3131* and *D16S408* (Fig. 2). One end of the shared region was defined by a recombination between *D16S3131* and *D16S3093* in individual III-3 in Family A, and the other end by a recombination between *D16S514* and *D16S408* in individual III-1 in the same family. These results defined a minimum PKCCR in the four new families within an approximately 24-cM segment between *D16S3131* and *D16S408*. Therefore, the present linkage/haplotype analysis did not contribute to narrow down the previously defined PKCCR.

Among a total of 1,563 exons of 157 genes analyzed, we detected 243 base alterations in the seven representative patients (Fig. 3), 36 of which were base substitutions in coding regions and have not been reported in the dbSNP database (<http://www.ncbi.nlm.->

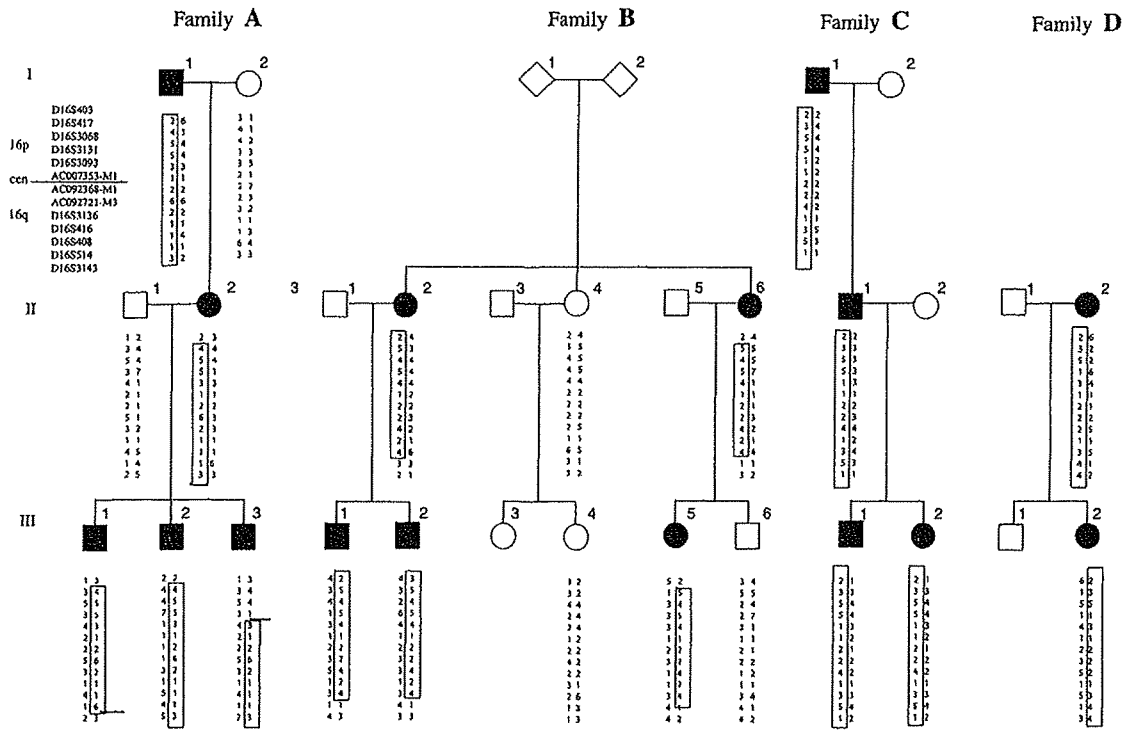


**Fig. 2** Haplotype analysis of the four new PKC families (Families A–D). The numbers in boxes represent putative disease haplotypes. The heavy short lines indicate recombination sites

nih.gov/SNP/). Seven of the alterations in six genes were nonsynonymous substitutions resulting in amino-acid substitutions (Table 2). Five of such nonsynonymous substitutions in four genes were observed both in some patients and among 100 normal control individuals. The remaining two, i.e., 6186C>A in exon 3 of *SCNN1G* (the gene for sodium channel, nonvoltage-gated 1, gamma) and 45842A>G in exon 29 of *ITGAL* (the integrin alpha L precursor gene), observed in Families C and F, respectively, were not observed among more than 400

normal controls. The real-time quantitative PCR analysis did not detect a duplication or a deletion within the two genes. Of the 35 intronic base changes we identified in the seven patients, none were located at the acceptor or donor splice sites (Fig. 3).

G-banding chromosome analysis at the 400-band level and C-banding analysis revealed that all five patients from Families B–D, F, and G had a normal-sized heterochromatin block on chromosome 16 without an inversion (data not shown).

**Fig. 3** Classification of 243 base alterations in 157 candidate genes. Information of the newly found single nucleotide polymorphisms (SNPs) is shown in Table 2. None of the novel intronic SNPs are located at any of the acceptor or donor splice sites

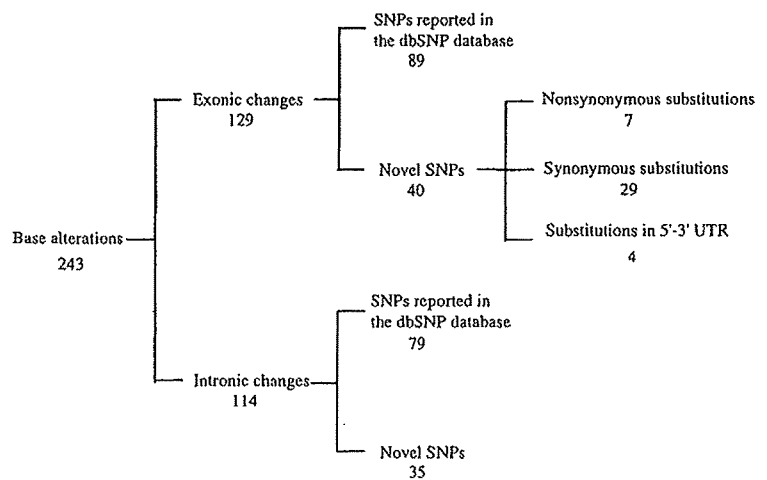


**Table 2** List of genes for mutation analysis in the PKC patients, and novel SNPs identified, their positions, nucleotide changes, and amino acid changes

Gene	E/I	SNP definition	AA	Gene	E/I	SNP definition	AA	Gene	E/I	SNP definition	AA
HS3ST2*				ASPHD1	E1	515insTGG		ITGAX*			
SCNN1G*	E3	6185G>T	Y241Y	KCTD13*	I2	INV2-74A>T		ITGAD*	5'U	5'U-13G>C*	
	E3	6186C>A	P242T	LOC124446					E2	943C>T	G33G
SCNN1B*				TAOK2*					I7	INV7+38C>T	
UBPH*				HIRIP3*					E8	14188A>G	R246R
NDUFAB1*				CCDC95					E8	14253A>G	Y268C
PRKCB1*	E1	79C>A	R27R	DOC2A*					I9	INV10-43G>A	
	I15	INV15+85G>T		FAM57B	I2	INV2+66G>T			E16	19819A>G	S644G
CACNG3*				ALDOA*					I17	INV17+139G>A	
TNRC6A*	E1	5'U-12079T>A		PPP4C*	E1	5'U-355-347del(CGG)3			I19	INV19+71C>T	
	E21	33511C>T	H1551H	TBX6*					I27	INV27+87G>A	
SLC5A11*	I1	5'U-12193T>C		YPEL3*				ARMC5*			
	I2	INV2+6C>G		GDPD3				TGFB111*	E5	753C>T	P119S
	I5	INV5-30G>A		MAPK3*				SLC5A2*			
	I5	INV5+65T>C		CORO1A*				Cl6orf58*	I5	INV5+53G>A	
LCMT1*				SULT1A3*				ERAF*	3'U	3'U+570T>C*	
IL4R*	I3	INV3+72T>A		CD2BBP2*	I1	INV1+493C>T		MGC3020*			
	E11	22448T>C	L433L	TBC1D10B*				ZNF720*			
IL21R*	I4	INV4+51C>T		MYLFP	I5	INV5+27G>A		ZNF267			
GTF3C1*				SEPT1*				TP53TG3*	E3	1232insG	
KIAA0556*	I16	INV16+4T>C		ZNF553	E2	2434G>A	T326T	FLJ43855			
	E18	204044A>G	Q1198Q	ZNF771				POL3S			
GSGIL*				XTP3TPA*				FLJ46121			
XPO6*	I9	INV9+31insT		SEPHS2*				FLI43980	E1	5'U-15C>G	
	I15	INV15+23G>C		ITGAL*	E1	5'U-86C>T		SHCBP1*	E5	12986C>T	N204N
	E16	69120T>C	N740N		E29	45842A>G	K1063R	VPS35*			
SBK-1				ZNE768				ORCGL	E6	6328A>G	V193V
LOC440350				ZNF747				MLCK*			
LOC440348				ZNF764				LOC388272*			
CLN3*	I12	INV12+36C>T		ZNF688				GPT2*			
	E15	14138A>G	H404R	ZNF785				DNAJA2*			
APOB48R*				ZNF689				NETO2*	I3	INV3-34G>A	
IL27*	I5	INV5-12C>T		PRR14				ITFG1*			
NUPR1*				FBS1*				PHKB*	I28	INV28+37C>T	
CCDC101*				SRCAP*				ABCC12*			
SULT1A2*				PHKG2*				ABCC11*			
SULT1A1*				LOC90835				LONPL*			
EIF3S8*	E16	20499C>T	P725P	RNF40*				SIAH1			
ATXN2L*	I13	INV13+55G>A		BCL7C*				N4BP1*			
TUFM*				CTF1*				CBLN1*			
SH2B*				LOC283932				FLJ44674	E1	3'U+905C>G	
ATP2A1*				FBXL19*				Cl6orf78*	E1	45G>A	K15K
RABEP2*	I3	INV4-56C>T		TMEM142C					I3	INV3+27A>G	
CD19*	E4	1379G>T	P206P	SETD1A*				ZNF423*			
SPIN1*	E7	6897C>T	S319S	HSD3B7*				Cl6orf69			
	I7	INV7+278Cdel		STX1B2*				HEATR3*	I11	INV11-44A>G	
	3'U	3'U+9285C>A*		STX4A*	I8	INV8+55C>A		PAPD5*			
LAT	E7	1259G>A	A120A		I8	INV8+65C>T		ADCY7*	E22	24951T>C	Y875Y
BOLA2				ZNF668				BRD7*	I9	INV9-26insT	
GDYD1*				ZNF646*	I1	5'U-108T>G			E16	48481G>A	T570T
SPN*					E2	2722G>C	G907A	NKD1*			
QPR1*				VKORC1*	3'U	3'U+3730G>C*		SLIC1*			
Cl6orf54				BCKDK*				CARD15*			
KIF22*	I12	INV12+70A>G		MYST1*				CYLD*	E17	43909C>T	D805D
MAZ*				PRSS8*	E3	2163C>T	V46V	SALL1*			
PRRT2				PRSS36				FTS*			
MVP*	E10	11504C>T	D525D	FUS*				CAPNS2*			
Cl6orf53				TRIM72				SLC6A2*			
CDIPT*				PYCARD*				GNAO1*			
PSK-1*				PYDC1*				CNGB1*	E22	51134C>T	N725N
				ITGAM*	I2	INV2+11T>C					

A total of 75 SNPs not reported in the dbSNP database were found in this study

Four SNPs found in 5'-UTR or 3'-UTR happened to be included in the sequenced regions

\*Analyzed in seven representative patients: E/I=exon or intron; AA=inferred amino acid change from nonsynonymous SNP; U=UTR

**Fig. 4** The PKC-critical region (PKCCR) summarized by five mapping studies (Tomita et al. 1999; Bennett et al. 2000; Swoboda et al. 2000; Cuenca-Leon et al. 2002, present study), as well as a seemingly second PKC locus (EKD2) by Valente et al. (2000). The location of markers and intermarker distances are from the Généthon map (Dib et al. 1996)

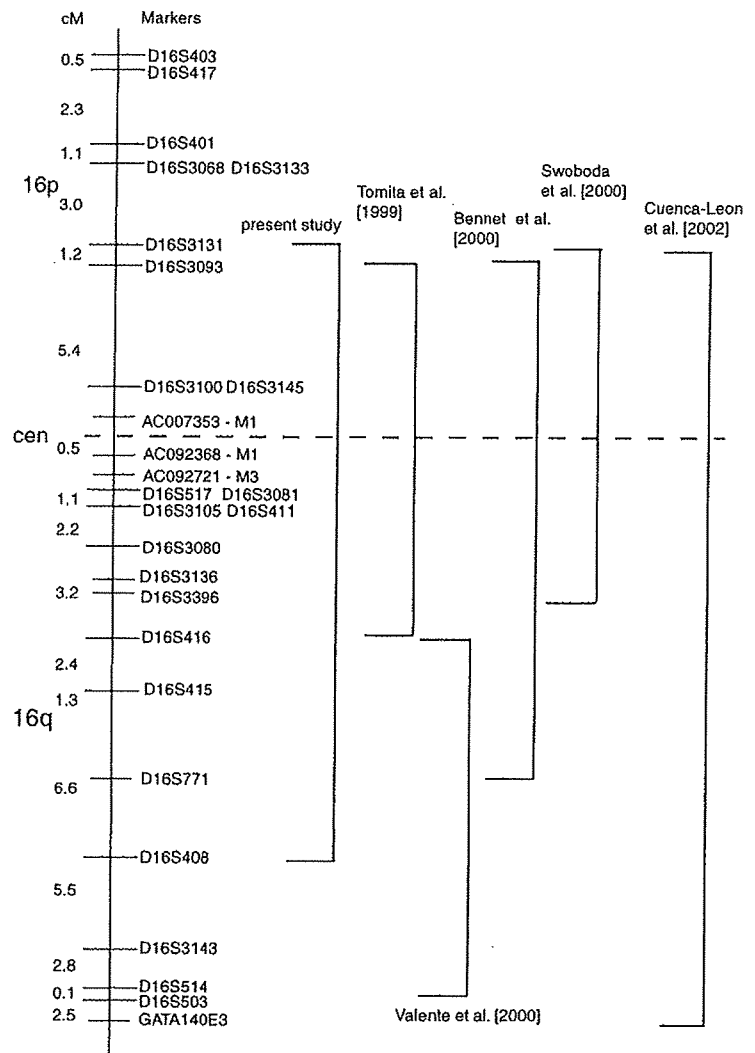


**Table 3** List of exons that have not been sequenced in the mutation analysis

Gene	Exon
<i>COX6A2</i>	Exon 2, Exon 3
<i>MAZ</i>	Exon 1, Exon 2, Exon 3
<i>VPS35</i>	Exon 9, Exon 10, Exon 11
<i>SULT1A1</i>	Exon 7
<i>SALL1</i>	Exon 2
<i>MGC2474</i>	Exon 2
<i>FLJ43855</i>	Exon 5, Exon 7, Exon 9

**Discussion**

The PKCCR was assigned to a segment between *D16S3093* and *D16S416* in eight Japanese families (Tomita et al. 1999). It was also mapped between *D16S3100* and *D16S771* in an Afro-Caribbean family (Bennett et al. 2000), between *D16S3131* and

*D16S3396* in 11 families of diverse ethnicity (Swoboda et al. 2000), between *D16S3145* and *GATA140E03* in a Spanish family (Cuenca-Leon et al. 2002), and a 24-cM segment between *D16S3131* and *D16S408* in the present study (Fig. 4). Thus, the shortest region of overlap (SRO) did not become narrower than a 12.4-cM segment detected by Tomita et al. (1999). Valente et al. (2000) assigned a form of PKC (a second PKC locus, EKD2), in an Indian family, to a segment between *D16S416* and *D16S503*, the region distinct from those mapped by Tomita et al. (1999) and by Swoboda et al. (2000). Furthermore, two other clinical entities, ICCA and BFIC2, were assigned to a region encompassing the centromere of chromosome 16 (Lee et al. 1998; Hattori et al. 2000; Swoboda et al. 2000; Caraballo et al. 2001; Weber et al. 2004). Since all of these loci were confined to a relatively small region, it is likely that all of these paroxysmal movement dis-

orders actually belong to one disorder and are allelic, as suggested previously (Tomita et al. 1999).

We searched for mutations in almost all protein-coding genes mapped at the PKCCR. In addition, we also analyzed four ion-channel-related genes (*CACNG3*, *SCNN1B*, *SCNN1G*, and *CNGBI*), albeit located outside the PKCCR, since many episodic neurologic disorders, such as muscle diseases, epilepsy, and movement disorders, are known as ion-channel abnormalities (Bhatia et al. 2000). However, 14 coding exons in seven genes (Table 3) were not analyzed because of difficulties in PCR-amplification.

In the present study on a total of 157 genes, we failed to identify any causative mutations that can explain PKC in all of the seven families examined. However, two nonsynonymous substitutions, 6186C>A in exon 3 of *SCNN1G* and 45842A>G in exon 29 of *ITGAL*, which were co-segregated with PKC in Families C and F, respectively, which were not found in normal control individuals, might be implicated in PKC. In other words, they were not able to be totally ruled out from the candidacy for PKC. It thus remains to be investigated whether another mutation in either gene is found in other PKC families.

Although the mapping of PKC was successful in at least nine studies, causative mutations have been uncovered. This may imply that PKC is caused by aberrations other than exonic mutations, such as a deletion or insertion, in the promoter regions, including the 5'-UTR or 3'-UTR. However, there is still a possibility for usual exonic mutations in a novel gene not annotated in public databases. As PKC itself is, generally, a viable disorder with which patients may show high reproductive fitness, such a mutated allele may be transmitted through many generations. A chromosomal rearrangement is another possibility. The pericentromeric region of chromosome 16 has a large heterochromatin (C-band) block that contains several duplicated regions, through which, frequent chromosomal rearrangements occur (Loftus et al. 1999). It remains also to be seen whether PKC patients within a family share such a variant.

**Acknowledgments** We are indebted to the family members for their participation in this research. We especially thank Ms. Y. Noguchi and A. Goto for their technical assistance. N.N. was supported in part by a Grant-in-Aid for Scientific Research (Category S, grant no. 13854024; Priority Areas for Applied Genomics, grant no. 17019055) from the Ministry of Education, Culture, Sports, Science and Technology (MEXT) of Japan, and by Solution Oriented Research of Science and Technology (SORST) from the Japan Science and Technology Agency (JST). K.Y. was supported by a Grant-in-Aid for Scientific Research for Priority Areas (grant no. 17590288) from the MEXT of Japan.

## References

- Bennett LB, Roach ES, Bowcock AM (2000) A locus for paroxysmal kinesigenic dyskinesia maps to human chromosome 16. *Neurology* 54(1):125–130
- Bhatia KP (1999) The paroxysmal dyskinesias. *J Neurol* 246(3):149–155
- Bhatia KP, Griggs RC, Ptáček LJ (2000) Episodic movement disorders as channelopathies. *Mov Disord* 15(3):429–433
- Caraballo R, Pavak S, Lemainque A, Gastaldi G, Echenne B, Motte J, Genton P, Cersósimo R, Humbertclaude V, Fejerman N, Monaco AP, Lathrop MG, Rochette J, Szepletowski P (2001) Linkage of benign familial infantile convulsions to chromosome 16p12-q12 suggests allelism to the infantile convulsions and choreoathetosis syndrome. *Am J Hum Genet* 68(3):788–794
- Cuenca-Leon E, Cormand B, Thomson T, Macaya A (2002) Paroxysmal kinesigenic dyskinesia and generalized seizures: clinical and genetic analysis in a Spanish pedigree. *Neuropediatr* 33(6):288–293
- Dib C, Faure S, Fizames C, Samson D, Drouot N, Vignal A, Millasseau P, Marc S, Hazan J, Seboun E, Lathrop M, Gyapay G, Morissette J, Weissenbach J (1996) A comprehensive genetic map of the human genome based on 5246 microsatellites. *Nature* 380:152–154
- Hattori H, Fujii T, Nigami H, Higuchi Y, Tsuji M, Hamada Y (2000) Co-segregation of benign infantile convulsions and paroxysmal kinesigenic choreoathetosis. *Brain Develop* 22(7):432–435
- Kato N, Sadamatsu M, Kikuchi T, Niikawa N, Fukuyama Y (2006) Paroxysmal kinesigenic choreoathetosis: from first discovery in 1892 to genetic linkage with benign familial infantile convulsions. *Epilepsy Res* 70(Suppl 1):174–184
- Lee W-L, Tay A, Ong H-T, Goh L-M, Monaco AP, Szepletowski P (1998) Association of infantile convulsions with paroxysmal dyskinesias (ICCA syndrome): confirmation of linkage to human chromosome 16p12-q12 in a Chinese family. *Hum Genet* 103(5):608–612
- Loftus BJ, Kim UJ, Sneddon VP, Kalush F, Brandon R, Fuhrmann J, Mason T, Crosby ML, Barnstead M, Cronin L, Deslattes Mays A, Cao Y, Xu RX, Kang HL, Mitchell S, Eichler EE, Harris PC, Venter JC, Adams MD (1999) Genome duplications and other features in 12 Mb of DNA sequence from human chromosome 16p and 16q. *Genomics* 60(3):295–308
- Nagamitsu S, Matsuishi T, Hashimoto K, Yamashita Y, Aihara M, Shimizu K, Mizuguchi M, Iwamoto H, Saitoh S, Hirano Y, Kato H, Fukuyama Y, Simada M (1999) Multicenter study of paroxysmal dyskinesias in Japan—clinical and pedigree analysis. *Mov Disord* 14(4):658–663
- Sadamatsu M, Masui A, Sakai T, Kunugi H, Nanko S, Kato N (1999) Familial paroxysmal kinesigenic choreoathetosis: an electrophysiologic and genotypic analysis. *Epilepsia* 40(7):942–949
- Swoboda KJ, Soong B, McKenna C, Brunt ER, Litt M, Bale JF Jr, Ashizawa T, Bennett LB, Bowcock AM, Roach ES, Gerson D, Matsuura T, Heydemann PT, Nespeca MP, Jankovic J, Leppert M, Ptáček LJ (2000) Paroxysmal kinesigenic dyskinesia and infantile convulsions: clinical and linkage studies. *Neurology* 55(2):224–230
- Tomita H, Nagamitsu S, Wakui K, Fukushima Y, Yamada K, Sadamitsu M, Masui A, Konishi T, Matsuishi T, Aihara M, Shimizu K, Hashimoto K, Mineta M, Matsushima M, Tsujita T, Saito M, Tanaka H, Tsuji S, Takagi T, Nakamura Y, Nakano S, Kato N, Nakane Y, Niikawa N (1999) Paroxys-



- mal kinesigenic choreoathetosis locus maps to chromosome 16p11.2-q12.1. *Am J Hum Genet* 65(6):1688–1697
- Valente EM, Spacey SD, Wali GM, Bhatia KP, Dixon PH, Wood NW, Davis MB (2000) A second paroxysmal kinesigenic choreoathetosis locus (EKD2) mapping on 16q13-q22.1 indicates a family of genes which give rise to paroxysmal disorders on human chromosome 16. *Brain* 123(10):2040–2045
- Weber YG, Berger A, Bebek N, Maier S, Karafyllakes S, Meyer N, Fukuyama Y, Halbach A, Hikel C, Kurlemann G, Neubauer B, Osawa M, Püst B, Rating D, Saito K, Stephani U, Tauer U, Lehmann-Horn F, Jurkat-Rott K, Lerche H (2004) Benign familial infantile convulsions: linkage to chromosome 16p12-q12 in 14 families. *Epilepsia* 45(6):601–609

## A syndactyly type IV locus maps to 7q36

Daisuke Sato · Desheng Liang · Lingqian Wu · Qian Pan ·  
Kun Xia · Heping Dai · Hua Wang · Gen Nishimura · Koh-Ichiro Yoshiura ·  
Jiahui Xia · Norio Niikawa

Received: 26 March 2007 / Accepted: 2 April 2007 / Published online: 3 May 2007  
© The Japan Society of Human Genetics and Springer 2007

**Abstract** Syndactyly occurs as an isolated abnormality or a part of a malformation syndrome. Syndactyly types I, II, III and V have been mapped to chromosomal regions 2q34–q36, 2q31–q32, 6q21–q23.2 and 2q31–q32, respectively, whereas syndactyly type IV (SD4) is extremely rare, and its gene localization has not yet been assigned. The SD4 manifests complete syndactyly of all fingers accompanied with polydactyly, and flexion of the fingers gives

the hand a cup-shaped appearance. We performed a linkage and haplotype analysis of a Chinese pedigree with autosomal dominant, non-syndromic SD4 using a set of 406 microsatellite markers. The analysis gave the maximum two-point LOD score of 1.613 at recombination fraction of 0.00 and penetrance of 1.00. Thus, the SD4 locus in the family was likely assigned to a 17.39-cM region at a segment between markers D7S3070 and D7S559 at 7q36, although the LOD score obtained was not high enough to conclude the localization. Analysis of three candidate genes, *LMBR1*, *SHH* and *ZRS*, failed to identify any pathogenic mutations. Our gene mapping may give a clue to identify the putative SD4 gene and provide a better understanding of normal human limb development.

Daisuke Sato and Desheng Liang equally contributed to this study.

D. Sato · D. Liang · L. Wu · K.-I. Yoshiura · N. Niikawa  
Department of Human Genetics, Nagasaki University  
Graduate School of Biomedical Sciences, Nagasaki, Japan

D. Sato · D. Liang · L. Wu · K.-I. Yoshiura · N. Niikawa  
Solution Oriented Research of Science and Technology  
(SORST), Japan Science and Technology Agency (JST),  
Kawaguchi, Japan

D. Sato  
Department of Pediatrics, Hokkaido University Graduate  
School of Medicine, Sapporo, Japan

D. Liang · L. Wu (✉) · Q. Pan · K. Xia · H. Dai · J. Xia  
National Laboratory of Medical Genetics, Xiangya Hospital,  
Central South University, 110 Xiangya Road, Changsha,  
Hunan 410078, China  
e-mail: wulingqian@cnimg.com

H. Wang  
Women and Children's Hospital of Hunan Province,  
Changsha, China

G. Nishimura  
Department of Radiology, Tokyo Metropolitan Kiyose  
Children's Hospital, Tokyo, Japan

**Keywords** Syndactyly type IV · Linkage analysis ·  
Disease gene mapping

### Introduction

Syndactyly is one of the most frequent congenital limb abnormalities and occurs as an isolated anomaly or a part of a malformation syndrome. Syndactyly falls into five major types I–V based on different combinations of affected fingers and toes and showing an autosomal dominant mode of inheritance. Syndactyly type I (OMIM 185900), type II (OMIM 186000), type III (OMIM 186100) and type V (OMIM 186300) have been mapped to chromosomal regions 2q34–q36, 2q31–q32, 6q21–q23.2 and 2q31–q32, respectively. Among them, only type III syndactyly was suggested to be an allelic disorder of oculodentodigital dysplasia (ODDD, MIM 164200) that is caused by mutations in the gene for gap junction protein alpha-1 (GJA1). Genes responsible for other types of syndactyly have not been

identified. Syndactyly type IV (SD4, OMIM 186200) is extremely rare and has been reported only twice since the first description by Haas in 1940 (Gillesen-Kaesbach and Majewski 1991; Rambaud-Cousson et al. 1991). Patients with this disease have complete syndactylism of all the fingers accompanied with polydactyly and cup-shaped hands due to flexion of the fingers. The etiology of SD4 has remained unknown, and its gene localization has not yet been mapped.

We recently encountered a Chinese pedigree with autosomal dominant SD4. Herein we report on their clinical manifestations and genetic linkage study.

**Materials and methods**

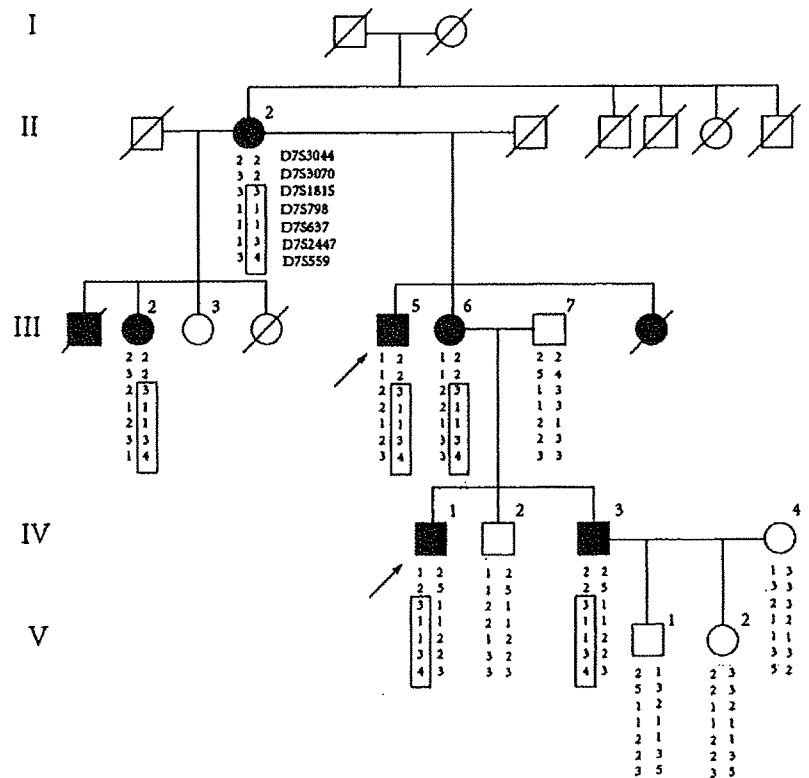
This study was approved by the Committee for Ethical Issues on Human Genome and Gene Analysis, Nagasaki University. We ascertained a five-generation non-consanguineous Chinese family with autosomal dominant, non-syndromic syndactyly (Figs. 1, 2). The family consisted of 23 members, including 8 affected individuals (4 females and 4 males). A total of 11 family members (6 affected and 5 unaffected individuals) were available for clinical evaluations and linkage and haplotype analyses.

All the patients examined were mentally normal, but had hand and/or foot anomalies. Individuals II-2, III-2 and III-6

had bilateral complete syndactyly with flexion of fingers, cup-shaped hands, polydactyly with two additional small and non-functional fingers at the edge of both hands, six metacarpals (Fig. 2a, b) and normal feet. In addition to the hand polysyndactyly, individuals III-5 and IV-1 had foot anomalies such as seventh and eighth toes on the left and right foot, respectively, and partial cutaneous syndactyly between toes two and three. Their excess toes existed on the tibial side of both feet, and lower extremities were bent and tubby, and showed tibial hemimelia. Knee and ankle joint malformations were present in III-5 and IV-1. Radiograph of the hands and left foot of III-5 showed six metacarpals (Fig. 2g), seven metatarsals and tibial hypoplasia (Fig. 2h), leading to a diagnosis of the disease in the family as Haas type (type IV) mirror-image polydactyly of hands and feet with tibial hypoplasia. III-5 (Fig. 2c–f) also had two triphalangeal thumbs bilaterally. Individual IV-3 presented with syndactyly of fingers two to six and toes five to six, stiffness of proximal interphalangeal joints in all his fingers and two additional small and non-functional fingers bilaterally. None of the five patients showed bone fusion radiologically.

DNA samples were extracted from peripheral blood leukocytes of the 11 members of the family after obtaining written informed consents. We carried out a whole-genome search except for the chromosome X. These individuals

**Fig. 1** Pedigree of a Chinese SD4 family with haplotypes at seven marker loci on chromosome 7. The number in the box depicts haplotype common to affected individuals



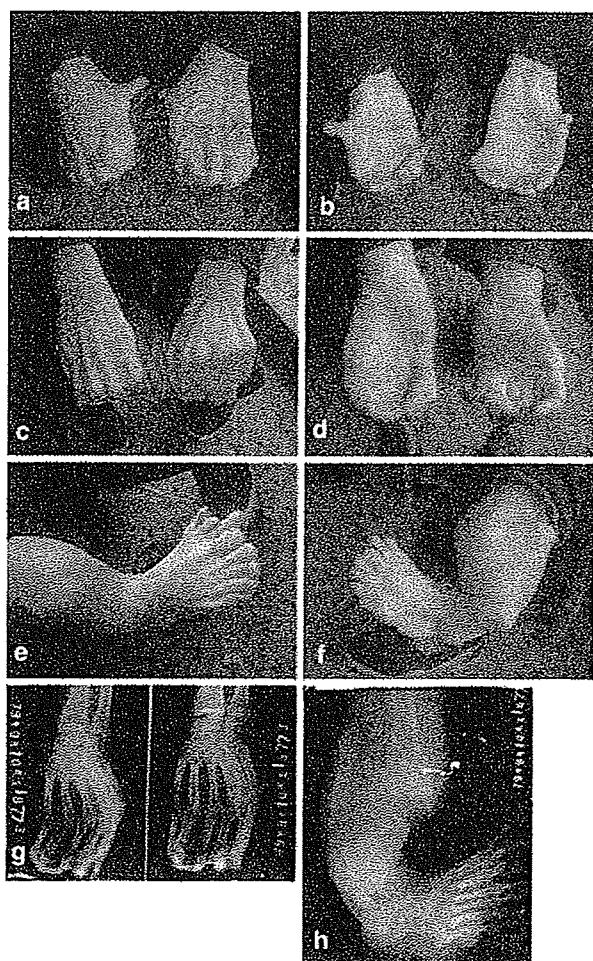


**Fig. 2** Hand/foot malformations of affected individuals. **a, b** Polysyndactyly of fingers in III-6. **c–f** Polysyndactyly of fingers and/or toes in III-5. **g, h** Radiograph of hands and left leg/foot in III-5, showing six metacarpals and seven metatarsals without bone fusion, and tibial hypoplasia

were genotyped at 406 microsatellite marker loci that are distributed with an average of 10-cM intervals over the whole genome. Two-point LOD scores were calculated using the MLINK program of the FASTLINK package, assuming that the disease in the family is inherited in an autosomal dominant mode with complete penetrance (penetrance = 1.00), the disease-allele frequency is 0.001 and allele frequencies are equal at all the marker loci.

A mutation screening in three candidate genes, *LMBR1* for limb region 1 protein, *SHH* for sonic hedgehog and *ZRS* for an *SHH* regulator, was performed in six affected individuals and two unaffected members of the family. All exon and flanking intron sequences of *LMBR1* and *SHH* and a 774-bp highly conserved sequence of *ZRS* were amplified by PCR for direct sequencing. PCR conditions were set at 40 cycles of 94°C for 30 s, 62°C for 30 s and at

72°C for 45 s in a 15- $\mu$ l mixture containing 1 $\times$  PCR buffer with 1.5 mM MgCl<sub>2</sub>, 0.2 mM each of dNTP, 1  $\mu$ M each primer and 0.4 units ExTaq DNA polymerase (TaKaRa, Otsu, Japan). PCR products were treated with ExoSAP-IT (AmershamBiosciences, Piscataway, NJ), and both strands of DNA were sequenced with BigDye Terminator Sequencing kit version 3.1 according to the supplied protocol (AppliedBiosystems, Foster City, CA). The reaction mixture was purified using Sephadex G-50 superfine (AmershamBiosciences) and analyzed on the ABI Genetic Analyzer 3100 (AppliedBiosystems) with the Sequence-Analysis software (AppliedBiosystems) and aligned with the AutoAssembler version 2.1.1 software (AppliedBiosystems) to find DNA alterations.

## Results and discussion

The disease in the Chinese family was clinically diagnosed as syndactyly type IV (SD4), because one (III-5) of the affected members had complete syndactylism of all fingers and toes accompanied with polydactyly. Flexion of fingers together with cutaneous syndactyly gave his hands a cup-shaped appearance. SD4 in the family was inherited as an autosomal dominant mode as was reported in the family with SD4 (Gillissen-Kaesbach and Majewski 1991; Rambaud-Cousson et al. 1991).

At an initial genotyping at the 406 marker loci, only seven members [five affected and two unaffected members (II-2, III-2 and 5–7, and IV-2 and 3)] were available. We obtained a possible linkage of the disease locus to five markers (*D2S2152*, *D7S559*, *D12S1052*, *D16S3039* and *D17S1822*) on chromosomes 2, 7, 12, 16 and 17 with LOD scores higher than 1.00. However, haplotype analysis excluded four of the five loci and retained *D7S559* as a candidate region for SD4 at 7q36.3. We then performed a second analysis by the use of more markers around 7q36.3 and by adding four more members (one patient IV-1 and three unaffected members IV-4, V-1 and V-2) who participated in the study later. The maximum two-point LOD score within the locus was 1.613 at recombination fraction of 0.00 and penetrance of 1.00 (Table 1). Haplotype analysis showed that all the six affected members had the same haplotype ‘‘3-1-1-3-4’’ for five marker loci, *D7S1815*, *D7S798*, *D7S637*, *D7S2447* and *D7S559* (Fig. 1). From these findings, it is most likely that SD4 in the Chinese family was assigned to a 17.39-cM region at 7q36, although the LOD score obtained was not high enough to conclude a concrete linkage. Direct sequencing of patients’ DNA for exon and flanking intron sequences of *LMBR1* and *SHH* and the conserved sequence of *ZRS* revealed no pathogenic mutation.

To a similar region where we assigned a SD4 locus, several forms of limb abnormalities have been mapped.

**Table 1** Two-point LOD score of chromosome 7q markers at various recombination fractions

Marker	Position (cM)	LOD score at theta (penetrance = 1.00)						
		0.00	0.05	0.10	0.15	0.20	0.25	0.30
D7S3044	153.7	-2.75	-0.480	-0.225	-0.096	-0.021	0.024	0.047
D7S3070	165.6	0.68	0.714	0.700	0.657	0.594	0.517	0.430
D7S1815	167.1	1.380	1.276	1.166	1.050	0.928	0.798	0.660
D7S798	169.9	0.861	0.796	0.728	0.657	0.581	0.500	0.415
D7S637	174.0	0.519	0.479	0.437	0.393	0.347	0.298	0.246
D7S2447	175.5	1.192	1.013	0.900	0.784	0.663	0.540	0.415
D7S559	183.0	1.613	1.446	1.271	1.090	0.902	0.712	0.526

They include preaxial polydactyly (Hing et al. 1995; Heus et al. 1999; Zguricas et al. 1999), complex polysyndactyly (Tsukurov et al. 1994), triphalangeal thumb (Heutink et al. 1994; Radhakrishna et al. 1996; Balci et al. 1999) and acheiropodia (Ianakiev et al. 2001). Among genes in the region, *LMBRI*, *SHH* and *ZRS* merit comments. It was shown that five point mutations residing in the highly conserved sequence of *ZRS* were associated with congenital preaxial polydactyly (Lettice et al. 2003; Gurnett et al. 2007), mutations in the chicken *Lmbri* are linked to chicken polydactyly (Huang et al. 2006), and *Shh* was responsible for the digit duplication activity in chick embryos (Riddle et al. 1993). Unfortunately, we failed to identify any pathogenic mutations of these genes in the SD4 patients from the Chinese family.

In conclusion, we have mapped the SD4 locus in the Chinese family to 7q36. This may become a clue to identify the gene responsible for this rare disease and provide a better understanding of normal human limb development.

**Acknowledgments** We are grateful to the patients and relatives for their participation in this study. N. Niikawa was supported in part by a Grant-in-Aid for Scientific Research (Priority Areas for Applied Genomics, no. 17019055) from the Ministry of Education, Culture, Sports, Science and Technology of Japan and by SORST from the Japan Science and Technology Agency (JST). L. Wu was supported by the Research Grant (30571201) from National Natural Science Foundation of China.

**Conflict of interest** The authors of this manuscript declare that they have no competing interests.

## References

- Balci S, Demirtas M, Civelek B, Piskin M, Sensoz O, Akarsu AN (1999) Phenotypic variability of triphalangeal thumb-polysyndactyly syndrome linked to chromosome 7q36. *Am J Med Genet* 87:399–406
- Gillesen-Kaesbach G, Majewski F (1991) Bilateral complete polysyndactyly (type IV Haas). *Am J Med Genet* 38:29–31
- Gurnett CA, Bowcock AM, Dietz FR, Morcuende JA, Murray JC, Dobbs MB (2007) Two novel point mutations in the long-range *SHH* enhancer in three families with triphalangeal thumb and preaxial polydactyly. *Am J Med Genet* 143:27–32
- Haas SL (1940) Bilateral complete syndactylism of all fingers. *Am J Surg*:363–366
- Heus HC, Hing A, van Baren MJ, Joosse M, Breedveld GJ, Wang JC, Burgess A, Donnis-Keller H, Berglund C, Zguricas J, Scherer SW, Rommens JM, Oostra BA, Heutink P (1999) A physical and transcriptional map of the preaxial polydactyly locus on chromosome 7q36. *Genomics* 57:342–351
- Heutink P, Zguricas J, van Oosterhout L, Breedveld GJ, Testers L, Sandkuijl LA, Snijders PJLM, Weissenbach J, Lindhout D, Hovius SER, Oostra BA (1994) The gene for triphalangeal thumb maps to the subtelomeric region of chromosome 7q. *Nat Genet* 6:287–291
- Hing AV, Helms C, Slaugh R, Burgess A, Wang JC, Herman T, Downton SB, Donnis-Keller H (1995) Linkage of preaxial polydactyly type 2 to 7q36. *Am J Med Genet* 58:128–135
- Huang YQ, Deng XM, Du ZQ, Qiu X, Du X, Chen W, Morisson M, Leroux S, Ponce de Leon FA, Da Y, Li N (2006) Single nucleotide polymorphisms in the chicken *Lmbri* gene are associated with chicken polydactyly. *Gene* 374:10–18
- Ianakiev P, van Baren MJ, Daly MJ, Toledo SPA, Cavalcanti MG, Correa Neto J, Lemos Silveira E, Freire-Maia A, Heutink P, Kilpatrick MW, Tsipouras P (2001) Acheiropodia is caused by a genomic deletion in *c7orf2*, the human orthologue of the *Lmbri* gene. *Am J Hum Genet* 68:38–45
- Lettice LA, Heaney SJH, Purdie LA, Li L, de Beer P, Oostra BA, Goode D, Elgar G, Hill RE, de Graaff E (2003) A long-range *Shh* enhancer regulates expression in the developing limb and fin and is associated with preaxial polydactyly. *Hum Mol Genet* 12:1725–1735
- Radhakrishna U, Blouin JL, Solanki JV, Dhoriani GM, Antonarakis SE (1996) An autosomal dominant triphalangeal thumb: polysyndactyly syndrome with variable expression in a large Indian family maps to 7q36. *Am J Med Genet* 66:209–215
- Rambaud-Cousson A, Dudin AA, Zwaiter AS, Thalji A (1991) Syndactyly type IV/hexadactyly of feet associated with unilateral absence of the tibia. *Am J Med Genet* 40:144–145
- Riddle RD, Johnson RL, Laufer E, Tabin C (1993) Sonic hedgehog mediates the polarizing activity of the ZPA. *Cell* 75:1401–1416
- Tsukurov O, Boehmer A, Flynn J, Nicolai JP, Hamel BCI, Traill S, Zaleske D, Mankin HJ, Yeon H, Ho C, Tabin C, Seidman JG, Seidman C (1994) A complex bilateral polysyndactyly disease locus maps to chromosome 7q36. *Nat Genet* 6:282–286
- Zguricas J, Heus H, Morales-Peralta E, Breedveld G, Kuyt B, Mumcu EF, Bakker W, Akarsu N, Kay SPJ, Hovius SER, Heredero-Baute L, Oostra BA, Heutink P (1999) Clinical and genetic studies on 12 preaxial polydactyly families and refinement of the localisation of the gene responsible to a 1.9 cM region on chromosome 7q36. *J Med Genet* 36:32–40

---

**Quantitative Structure–Activity  
Relationship Analysis and Molecular  
Dynamics Simulation To Functionally  
Validate Nonsynonymous Polymorphisms  
of Human ABC Transporter ABCB1  
(P-Glycoprotein/MDR1)**

---

**Aki Sakurai, Yuko Onishi, Hiroyuki Hirano, Michel Seigneuret,  
Kazuya Obanayama, Gunwoo Kim, Ei Leen Liew,  
Toshiyuki Sakaeda, Koh-ichiro Yoshiura, Norio Niikawa,  
Minoru Sakurai, and Toshihisa Ishikawa**

Department of Biomolecular Engineering, Graduate School of  
Bioscience and Biotechnology, Tokyo Institute of Technology,  
Yokohama, Japan, Institut Cochin, Departement de Biologie  
Cellulaire, CNRS (UMR 8104), INSERM (U567), Université Paris 5,  
Paris, France, Center for Integrative Education of Pharmacy Frontier,  
Graduate School of Pharmaceutical Sciences, Kyoto University,  
Kyoto, Japan, Department of Human Genetics, Nagasaki University  
Graduate School of Biomedical Sciences, Nagasaki, Japan, and  
CREST, Japan Science and Technology, Kawaguchi, Japan

**Biochemistry<sup>®</sup>**

Reprinted from  
Volume 46, Number 26, Pages 7678–7693

## Articles

## Quantitative Structure–Activity Relationship Analysis and Molecular Dynamics Simulation To Functionally Validate Nonsynonymous Polymorphisms of Human ABC Transporter ABCB1 (P-Glycoprotein/MDR1)<sup>†</sup>

Aki Sakurai,<sup>‡</sup> Yuko Onishi,<sup>‡</sup> Hiroyuki Hirano,<sup>‡</sup> Michel Seigneuret,<sup>§</sup> Kazuya Obanayama,<sup>‡</sup> Gunwoo Kim,<sup>‡</sup> Ei Leen Liew,<sup>‡</sup> Toshiyuki Sakaeda,<sup>||</sup> Koh-ichiro Yoshiura,<sup>⊥,‡</sup> Norio Niikawa,<sup>⊥,‡</sup> Minoru Sakurai,<sup>‡</sup> and Toshihisa Ishikawa<sup>\*,‡</sup>

Department of Biomolecular Engineering, Graduate School of Bioscience and Biotechnology, Tokyo Institute of Technology, Yokohama, Japan, Institut Cochin, Département de Biologie Cellulaire, CNRS (UMR 8104), INSERM (U567), Université Paris 5, Paris, France, Center for Integrative Education of Pharmacy Frontier, Graduate School of Pharmaceutical Sciences, Kyoto University, Kyoto, Japan, Department of Human Genetics, Nagasaki University Graduate School of Biomedical Sciences, Nagasaki, Japan, and CREST, Japan Science and Technology, Kawaguchi, Japan

Received January 13, 2007; Revised Manuscript Received April 28, 2007

**ABSTRACT:** Several preclinical and clinical studies suggest the importance of naturally occurring polymorphisms of drug transporters in the individual difference of drug response. To functionally validate the nonsynonymous polymorphisms of ABCB1 (P-glycoprotein/MDR1) *in vitro*, we generated SNP variant forms (i.e., S400N, R492C, R669C, I849M, A893P, A893S, A893T, M986V, A999T, P1051A, and G1063A) and expressed them in Sf9 cells. The kinetic properties ( $K_m$  and  $V_{max}$ ) of those variants were analyzed by measuring the ATPase activity to obtain the ATPase profile for each variant toward structurally unrelated substrates. On the basis of the experimental data, we determined the substrate specificity of ABCB1 WT and its variants by the quantitative structure–activity relationship (QSAR) analysis method. While several SNP variants appeared to influence the substrate specificity of ABCB1, the nonsynonymous polymorphisms of 2677G > T, A, or C at amino acid position 893 (Ala > Ser, Thr, or Pro) have great impacts on both the activity and the substrate specificity of ABCB1. The A893P variant (2677G > C), a rare mutation, exhibited markedly high activity of ATPase toward different test compounds. Molecular dynamics (MD) simulation based on a three-dimensional structural model of human ABCB1 revealed that multiple kinks are formed in the intracellular loop between transmembrane domains 10 and 11 of the A893P variant (2677G > C) protein. The polymorphisms of 2677G, 2677T, and 2677A exhibit wide ethnic differences in the allele frequency, and these nonsynonymous polymorphisms are suggested to be clinically important because of their altered ATPase activity and substrate specificity toward different drugs.

Pharmacogenomics dealing with heredity and response to drugs is a part of science that attempts to explain the variability of one or another drug response and to search for the genetic basis of such variations or differences. As a means to implementing personalized medicine based on pharmacogenomic data, it is critically important to understand the molecular mechanisms underlying interindividual differences

in the drug response, namely, pharmacological effect vs side effect. The occurrence of individual variations in the drug response may involve many different causes, for example, genetic variations and/or expression levels of drug target molecules, including membrane receptors, nuclear receptors, signal transduction components, and enzymes, as well as those of drug metabolizing enzymes and, importantly, drug transporters.

Human ABCB1<sup>1</sup> (P-glycoprotein or MDR1) was identified because of its overexpression in cultured cancer cells associated with an acquired cross-resistance to multiple anticancer drugs (1, 2). ABCB1 is expressed not only in cancer cells but also in many normal tissues. For example, it is located in the apical domain of the enterocytes of the gastrointestinal tract (jejunum and duodenum) and limits the uptake and absorption of drugs and other substrates from the intestine into the systemic circulation by excreting

<sup>†</sup> This study was supported by the NEDO International Joint Research Grant program "International standardization of functional analysis technology for genetic polymorphisms of drug transporters" and a research grant (14370754) from the Japanese Society for the Promotion of Science.

\* Corresponding author. Phone: +81-45-924-5800. Fax: +81-45-924-5838. E-mail: tishikaw@bio.titech.ac.jp.

<sup>‡</sup> Tokyo Institute of Technology.

<sup>§</sup> Université Paris 5.

<sup>||</sup> Kyoto University.

<sup>⊥</sup> Nagasaki University Graduate School of Biomedical Sciences.

<sup>†</sup> CREST.

substrates into the gastrointestinal tract. In addition, ABCB1 is expressed in the endothelial cells lining the small vessels of the human cortex, in which the transporter appears to be concentrated within the luminal cellular compartment. The expression of ABCB1 on the luminal membrane of capillary endothelial cells of the brain restricts drug distribution into the central nervous system (3, 4). This function of ABCB1 appears to be very important for protecting the central nervous system from attack by toxic compounds.

To date, genetic variations of the human *ABCB1* gene have been most extensively studied (5). Hitherto, more than 50 SNPs and several insertion/deletion polymorphisms in the *ABCB1* gene have been reported (5–24). Preclinical and clinical studies have provided evidence for naturally occurring polymorphisms in ABCB1 and their effects on drug absorption, distribution, and elimination (25). Hoffmeyer et al. reported multiple polymorphisms in the *ABCB1* gene (6). One of those mutations in particular, a C-to-T variant at position 3435 in exon 26 of the *ABCB1* gene, was reportedly correlated with ABCB1 expression and function, whereas an association of the 3435C > T polymorphism with ABCB1 protein expression and function remains controversial. It has been suggested that the 2677G > T/3435C > T haplotype is of clinical importance (8, 10, 16, 26). In this regard, Kimchi-Sarfaty et al. have most recently reported that the haplotype polymorphism of 1236C > T/2677G > T/3435C > T might change the substrate specificity of ABCB1 (27). Currently available reports as well as the NCBI dbSNP database show a triallelic polymorphism of ABCB1 (2677G > T/A) and one rare mutation (2677G > C). At present, however, information is still limited regarding the functional impact of the genetic polymorphisms in the *ABCB1* gene. Detailed functional analysis *in vitro* may provide clear insight into the biochemical and therapeutic significance of genetic polymorphisms.

In the present study, we have undertaken an *in vitro* quantitative analysis to precisely evaluate functional changes associated with genetic polymorphisms of ABCB1. For this purpose, ABCB1 cDNA cloned from a human liver cDNA library was prepared, and several variant forms (i.e., S400N, R492C, R669C, I849M, A893S, A893T, A893P, M986V, A999T, P1051A, and G1063A) were generated by site-directed mutagenesis. We have functionally evaluated those variants by using the newly developed quantitative structure–activity relationship (QSAR) analysis technique. Furthermore,

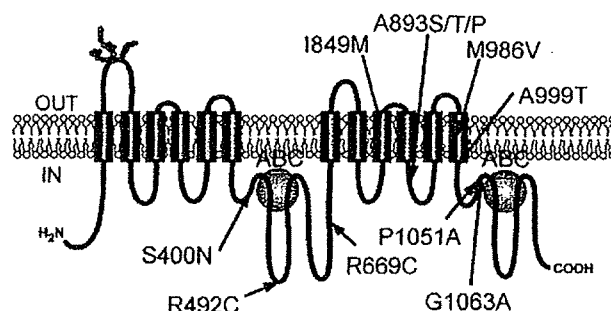


FIGURE 1: Schematic illustration of the human ABCB1 protein and positions of nonsynonymous SNPs that were functionally analyzed in the present study. SNP data were obtained from the NCBI dbSNP database and recent publications: S400N (6, 7, 29, 31); R492C (7); R669C (16); I849M (16); A893P (NCBI dbSNP, rs2032582); A893S (8, 16, 23, 29–31); A893T (8, 16, 23, 29–31); M986V (30); A999T (28); P1051A (16); G1063A (NCBI dbSNP, rs2707944). ATP-binding cassettes are indicated by ABC.

based on a putative three-dimensional structural model of human ABCB1, molecular dynamics (MD) simulation was carried out to gain more insight into the impact of nonsynonymous polymorphisms on structural changes that may affect the ATPase activity of ABCB1. Evidence is provided herein to show that nonsynonymous polymorphisms (2677G > T, A, or C) at amino acid position 893 (Ala > Ser, Thr, or Pro) have a great impact on both the activity and the substrate specificity of ABCB1.

## EXPERIMENTAL PROCEDURES

**Chemicals and Biochemicals.** The following compounds and therapeutic drugs were purchased from the commercial sources indicated in parentheses: ATP magnesium salt, sodium *o*-vanadate, epinephrine, norepinephrine,  $\gamma$ -aminobutyric acid (GABA), serotonin, melatonin, nifedipine, bepridil, fendiline, prenylamine, nicardipine, dexamethasone, prednisolone, cortisone, pinacidil, acetylsalicylic acid, indomethacin, acemetacin, ibuprofen, naproxen, mepirizole, vinblastine, etoposide, daunorubicin, paclitaxel, doxorubicin, 5-fluorouracil, quinidine, *p*-aminohippuric acid (PAH), penicillin G (benzylpenicillin), and novobiocin (Sigma-Aldrich Co., St. Louis, MO); glutamic acid, dopamine, histamine, verapamil, diltiazem, betamethasone, nicorandil, actinomycin D, and methotrexate (Wako Pure Chemical Industries, Ltd., Osaka, Japan); glycine, Tris, HEPES, EGTA, and EDTA (Nacalai Tesque, Inc., Kyoto, Japan); tacrolimus (Calbiochem, Darmstadt, Germany). All other chemicals were of analytical grade.

**SNP Data on Nonsynonymous Polymorphisms of the Human ABCB1 Gene.** SNP data on polymorphisms of the *ABCB1* gene were obtained from the NCBI dbSNP database ([http://www.ncbi.nlm.nih.gov/SNP/snp\\_ref.cgi?locusId=5243](http://www.ncbi.nlm.nih.gov/SNP/snp_ref.cgi?locusId=5243)) and recent publications (6–8, 16, 23, 28–31). Figure 1 illustrates the positions of the nonsynonymous polymorphisms of ABCB1 that were functionally analyzed in the present study.

**Preparation of Plasmids Carrying ABCB1 Variants.** Wild-type (WT) ABCB1 cDNA (NCBI NM\_000927.3) was inserted into the pFastBac1 plasmid as described previously (32). Nonsynonymous SNP variants were generated by using the QuikChange site-directed mutagenesis kit (Stratagene, La Jolla, CA). Polymerase chain reaction (PCR) was carried

<sup>1</sup> Abbreviations: ABC, ATP-binding cassette; cDNA, complementary DNA; CFC, chemical fragmentation code; ATP, adenosine triphosphate; EDTA, ethylenediaminetetraacetic acid; AMBER, assisted model building and energy refinement; EGTA, ethylene glycol bis( $\beta$ -aminoethyl ether)-*N,N,N',N'*-tetraacetic acid; FCS, fetal calf serum; GABA,  $\gamma$ -aminobutyric acid; HEPES, 2-[4-(2-hydroxyethyl)-1-piperazinyl]ethanesulfonic acid; HRP, horseradish peroxidase; IgG, immunoglobulin G;  $K_m$ , Michaelis–Menten constant; MD, molecular dynamics; MDR, multidrug resistance; MES, 2-(*N*-morpholino)ethanesulfonic acid; NCBI, National Center for Biotechnology Information; NSAID, non-steroidal antiinflammatory drug; PAH, *p*-aminohippuric acid; PBS, phosphate-buffered saline; PCR, polymerase chain reaction; QSAR, quantitative structure–activity relationship; RMSF, root-mean-square fluctuation; SAR, structure–activity relationship; SDS–PAGE, sodium dodecyl sulfate–polyacrylamide gel electrophoresis; SD, standard deviation; SNP, single nucleotide polymorphism; TM, transmembrane domain; Tris, tris(hydroxymethyl)aminomethane; TBS, Tris-buffered saline; TTBS, Tris-buffered saline containing 0.05% (v/v) Tween 20;  $V_{max}$ , maximum velocity; WT, wild type.



Table 1: Data on Oligonucleotide Primers Used for Site-Directed Mutagenesis and Experimental Conditions<sup>a</sup>

SNP		F/R primers	primer sequence (5' → 3')	primer length (bases)	% GC	T <sub>m</sub> (°C)
amino acid	cDNA					
S400N	1199G > A	F	CAGAAATGTTCACTTCAATTACCCATCTCGAAAAG	35	36.5	77.2
		R	CTTTTCGAGATGGGTAATGGAAGTGAACATTTCTG	35	36.5	77.2
R492C	1474C > T	F	TGAAAACATTCGCTATGGCTGTGAAAATGTCACCATGG	38	42.1	81.0
		R	CCATGGTGACATTTTCAACGCCATAGCGAATGTTTCA	38	42.1	81.0
R669C	2005C > T	F	TCTAATAAGAAAAAGATCAACTTGTAGGAGTGTCCGTGGATC	42	37.9	80.9
		R	GATCCACGGACACTCCTACAAGTTGATCTTTTCTTATTAGA	42	37.9	80.9
I849M	2547A > G	F	GGGACAGGAATAATTATGTCTTCATCTATGGTTGGCA	38	34.5	77.9
		R	TGCCAACCATAGATGAAAGGACATAATTATTCCTGTCCC	38	34.5	77.9
A893P	2677G > C	F	AGAAAGAAGTCTAGAGGCTTGGGAAGATCGCTAC	34	47.1	80.9
		R	GTAGCGATCTTCCCAGGACTTCTAGTTCCTTCT	34	47.1	80.9
A893S	2677G > T	F	GAAAGAAGTCTAGAGGCTTGGGAAGATCGCTAC	33	45.4	79.6
		R	GTAGCGATCTTCCCAGGACTTCTAGTTCCTTCT	33	45.4	79.6
A893T	2677G > A	F	GAAAGAAGTCTAGAGGCTTGGGAAGATCGCTAC	33	45.4	79.6
		R	GTAGCGATCTTCCCAGGACTTCTAGTTCCTTCT	33	45.4	79.6
M986V	2956A > G	F	GTCTTTGGTGCCGTGGCCGTGGGGC	25	73.8	84.7
		R	GCCCCACGGCCACGGCACCAAGAC	25	73.8	84.7
A999T	2995G > A	F	GTTCAATTTGCTCCTGACTATACCAAAGCCAAAATATCAGCAG	42	40.5	82.0
		R	CTGCTGATATTTGGCTTTGGTATAGTCAGGAGCAAATGAAC	42	40.5	82.0
P1051A	3151C > G	F	CGACCGGACATCGCAGTGCCTCAGGG	26	60.0	80.1
		R	CCCTGAAGCACTCCGATGTCCGGTCG	26	60.0	80.1
G1063A	3188G > C	F	GAGGTGAAGAAGGCCAGACGCTGGCTC	28	64.3	83.7
		R	GAGCCAGCGTCTGGCCCTTCTCACCTC	28	64.3	83.7

<sup>a</sup> F, forward; R, reverse. Sites of mutagenesis are indicated by underbars. The % GC indicates the percentage of guanine and cytosine contents in the PCR primers. T<sub>m</sub> shows the melting temperature for each PCR primer set.

out in an iCycler (Bio-Rad Laboratories, Inc., Hercules, CA) by using PfuTurbo DNA polymerase, the ABCB1-pFastBac1 plasmid, and specific primers (see Table 1 for primer sequences). The PCR was initiated with incubation at 94 °C for 2 min and then followed by 12 cycles of reactions at 94 °C for 30 s, at 55 °C for 30 s, and at 68 °C for 18 min. After the PCR, the reaction mixture was incubated with *DpnI* endonuclease at 37 °C for 1 h to digest the original template plasmid. Each variant cDNA generated in the pFastBac1 plasmid was subjected to nucleotide sequence analysis (Hitachi, Ltd., Tokyo, Japan).

**Expression of ABCB1 WT and SNP Variants in Insect Sf9 Cells.** Competent DH10Bac *Escherichia coli* cells were transformed by the variant ABCB1 plasmids. Then, the variant ABCB1 cDNA was transposed into the bacmid, which is the baculovirus' genome, in DH10Bac cells with the help of a helper plasmid. The recombinant bacmid was isolated and purified by using a QIAprep Spin Miniprep kit (Qiagen K.K., Tokyo, Japan).

Insect *Spodoptera frugiperda* (Sf9) cells were grown in EX-CELL 420 medium (JRH Biosciences, Inc., Lenexa, KS) supplemented with 1% (v/v) fetal calf serum (FCS) and 1% (v/v) antibiotic-antimycotic (Invitrogen Co., Carlsbad, CA) with gentle shaking at 27 °C. Sf9 cells were then transfected with the ABCB1-recombinant bacmid in the presence of Cellfectin reagent (Invitrogen Co., Carlsbad, CA) according to the manufacturer's protocol. Ninety-six hours after the transfection, the culture medium containing recombinant baculoviruses was harvested by centrifugation. To amplify the recombinant baculoviruses, Sf9 cells were further infected with the harvested virus and maintained for 72 h, after which the culture medium was harvested by centrifugation. This process was repeated three times.

To detect ABCB1 or its variants expressed in Sf9 cells, samples of the culture medium were taken, and 2.0 × 10<sup>6</sup> cells in the medium were rinsed with phosphate-buffered

saline (PBS) and collected by centrifugation. A 1 mL syringe with a 27 G needle was then used to homogenize the cells in 100 μL of cell lysis buffer containing 50 mM Tris-HCl (pH 7.4), 1% (v/v) Triton X-100, 1 mM dithiothreitol, and protease inhibitor cocktail (Nacal Tesque, Inc., Kyoto, Japan). Subsequently, the homogenate was centrifuged at 800g at 4 °C for 5 min. The resulting supernatant was collected, and the protein concentration was measured with a BCA protein assay reagent kit (Pierce Biotechnology, Inc., Rockford, IL).

**Immunoblot Analysis for Detection of ABCB1 WT and Its Variants.** The supernatant (10 μg of protein) was subjected to sodium dodecyl sulfate–polyacrylamide gel electrophoresis (SDS–PAGE). The separated proteins were subsequently transferred to a nitrocellulose membrane (Hybond ECL; Amersham Biosciences Corp., Piscataway, NJ). Following an incubation with 5% skim milk in Tris-buffered saline (TBS) at room temperature for 60 min, the nitrocellulose membrane was incubated with ABCB1-specific monoclonal antibody C219 (1:100 dilution; Calbiochem, Darmstadt, Germany) in Tris-buffered saline containing 0.05% (v/v) Tween 20 (TTBS) at room temperature for 90 min. Afterward, the nitrocellulose membrane was incubated with an anti-mouse IgG–horseradish peroxidase (HRP) conjugate (Cell Signaling Technology, Beverly, MA) diluted to 1:3000 in TTBS. HRP-dependent luminescence was developed by using the Western Lightning Western Blot Chemiluminescence Reagent Plus kit (Perkin-Elmer Life Sciences, Inc., Boston, MA). The chemiluminescence was detected in a Lumino Imaging Analyzer FAS-1000 (Toyobo Co., Ltd., Osaka, Japan), and the intensity was quantified by using a Gel Pro Analyzer v-3.1 (Toyobo Co., Ltd., Osaka, Japan).

**Preparation of Plasma Membrane.** Sf9 cells (1 × 10<sup>6</sup> cells/mL) were infected with the ABCB1-recombinant baculovirus. Plasma membrane fractions were prepared from Sf9 cells as described previously (32). Briefly, seventy-two hours after

infection, the cells were collected by centrifugation at 300g at 4 °C for 5 min and rinsed with PBS. The cells were homogenized with a Potter-Elvehjem homogenizer in hypotonic buffer (0.5 mM Tris-HEPES, 0.1 mM EGTA, pH 7.4). After centrifugation at 9100g at 4 °C for 10 min, the supernatants were pooled and centrifuged at 100000g at 4 °C for 30 min. The resulting precipitate was homogenized with a Potter-Elvehjem homogenizer in 10 mL of 0.25 M sucrose and 10 mM Tris-HEPES solution (pH 7.4). This mixture was layered over a 40% (w/v) sucrose solution containing 10 mM Tris-HEPES (pH 7.4) and then centrifuged at 100000g at 4 °C for 30 min. The turbid layer at the interface was collected and mixed with 10 mL of 0.25 M sucrose solution containing 10 mM Tris-HEPES (pH 7.4). The mixture was centrifuged at 100000g at 4 °C for 30 min. The resulting precipitate was suspended in a small volume of 0.25 M sucrose solution containing 10 mM Tris-HEPES (pH 7.4).

**Measurement of ABCB1 ATPase Activity.** The ATPase activity of ABCB1 and its variants in the Sf9 plasma membrane fraction was measured in the presence of various test compounds in 96-well plates, as described previously (32, 33). Cell membranes (2 µg of protein per well) were suspended in 10 µL of the incubation medium containing 50 mM Tris-MES (pH 6.8), 2 mM EGTA, 2 mM dithiothreitol, 50 mM potassium chloride, 5 mM sodium azide, and 2 mM ouabain (33). This medium was mixed with 10 µL of a test compound solution and then preincubated at 37 °C for 3 min. The ATPase reaction was started by adding 20 µL of 4 mM ATP/Mg solution to the reaction mixture, and the incubation was maintained at 37 °C for 30 min. The reaction was stopped by the addition of 20 µL of 5% trichloroacetic acid followed by 42 µL of solution A (2 M hydrochloric acid:0.1 M sodium molybdate = 4:3) and 18 µL of solution B [0.084% (w/v) malachite green in 1% (w/v) polyvinyl alcohol solution]. Thereafter, 120 µL of solution C [7.8% (v/v) sulfuric acid] was added to the mixture. These mixing processes were automatically carried out in a HALCS-I system (BioTec Co. Ltd., Tokyo, Japan). One hour after incubation at room temperature, the absorbance of each reaction mixture in the 96-well plates was photometrically measured at a wavelength of 630 nm in a Multiskan JX system (Dainippon Pharmaceuticals Co., Osaka, Japan). The amount of liberated phosphate was quantified on the basis of the calibration line established with inorganic phosphate standards. Throughout this study, we measured drug-stimulated ATPase activities (vanadate-sensitive) that were observed in ABCB1-expressing membrane preparations (see Results).

**QSAR Analysis Using Chemical Fragmentation Codes.** To perform the QSAR analysis for the functional validation of nonsynonymous polymorphisms of ABCB1 in this study, we generated the chemical fragmentation codes (CFCs) of all of the test compounds by using the Markush TOPFRAG program (<http://scientific.thomson.com/support/patents/patinf/terms/>). The CFCs are a set of alphanumeric symbols, each representing a fragment of a chemical structure. The Markush TOPFRAG program is a tool for searching the chemical structures and structure information in Derwent's online databases (<http://www.biobyte.com/bb/prod/40manual.pdf>). In the present study, we have formulated the extent of drug-stimulated ATPase activity of ABCB1 as a linear combina-

tion of CFCs, each of which was weighted by the corresponding coefficient,  $C(i)$ , as follows: where the symbol (i)

$$\text{drug-stimulated ATPase activity of ABCB1} = \sum C(i) \times \text{score}(i) + \text{constant}$$

designates a specific CFC. The "score" means the presence ( $\geq 1$ ) or absence (0) of the corresponding CFC in the chemical structure of a test compound. On the basis of the CFCs thus obtained and in comparison with the observed inhibition of transport activity for each test compound, we have calculated chemical fragmentation coefficients,  $C(i)$ , by multiple linear regression analysis, as described previously (34).

**Homology Modeling of the ABCB1 3D Structure.** An alignment of the sequence of human ABCB1 with twice that of the *Staphylococcus aureus* Sav1866 monomer was generated automatically with the ClustalX program (35) and optimized manually. Ambiguities occurred only in the alignment of the first, fifth, and sixth TM regions of each transporter half. These were resolved in each case by carrying out homology modeling with the different possible alignments and choosing the one that yielded no polar residue at the surface of the hydrophobic TM region of the final structure. The final alignment corresponds respectively to a 29% and 27% identity of the ABCB1 first and second transporter half with the Sav1866 monomer.

Homology modeling was performed with Modeller 7.7 (36). The first stage of modeling was done with the "model" routine using the Sav1866 dimer crystal structure (ref 37; PDB code 2HYD) as template. The 627–693 linker region of ABCB1 was not considered in the present study since it apparently bears no structural relevance to function apart from a flexibility requirement (38). Twenty-five structures were generated, and one was chosen, corresponding to a low value of the Modeller convergence function and to stereochemically adequate bond angles, bond lengths, and backbone dihedrals. In a second stage, the Modeller 7.7 "loop" routine (39) was used to optimize the conformations of nonaligned loops. All loops were optimized together. Fifty structures were generated, and one was chosen, corresponding to the major conformation of the large first extracellular loop and to an overall adequate bond and angle stereochemistry of all modeled loops. This final structure was quality-checked with WHAT IF (40) and PROCHECK (41). Ramachandran analysis indicated that 99.4% of the residues' backbone dihedrals were in allowed regions. Bond angle and length Z-scores were found to be satisfactory, and only minor steric clashes ( $<0.36$  Å) were detected.

**MD Simulation.** The initial three-dimensional structure of each variant protein (A893S, A893T, or A893P) was deduced from the ABCB1 structure template by using the LEAP module in the AMBER (assisted model building and energy refinement) simulation package. MD simulation was performed for those three-dimensional structure models by using the AMBER version 8.0 simulation program that had been developed by Case et al. (42). In the MD simulation, we used the force field parameter set of ff03 and represented the solvent as a generalized Born solvent model (43). Briefly, all atoms in each system were first minimized for 12000 steps by using the steepest descent algorithm to remove close contacts and to relax the system. Next, each system was

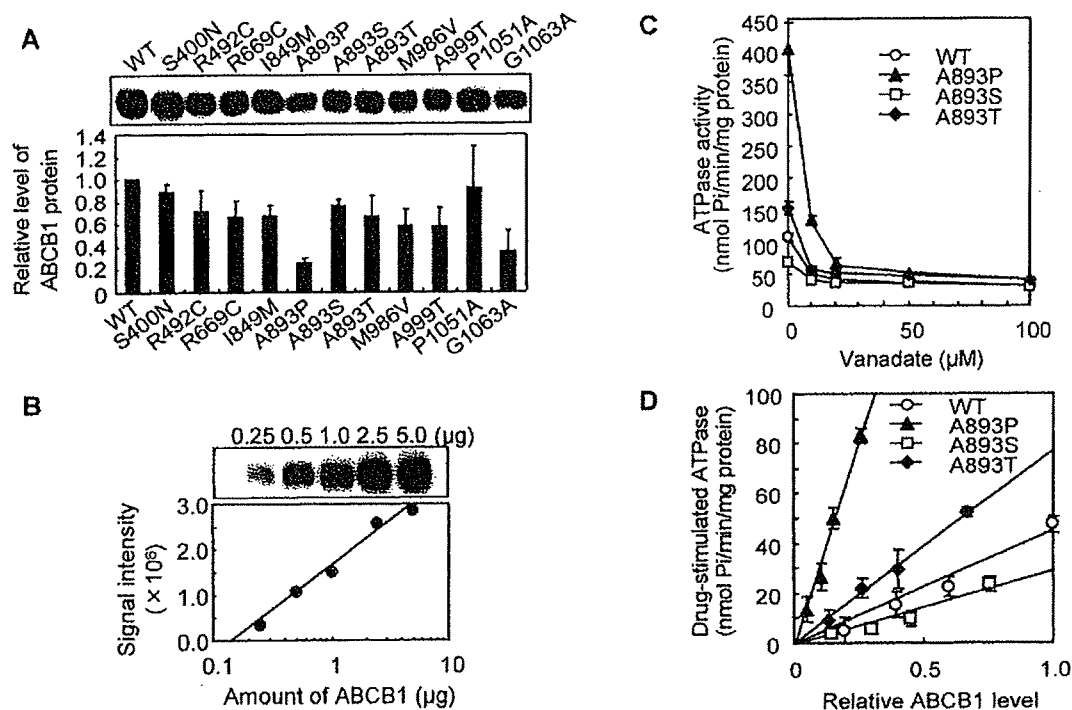


**FIGURE 2:** Immunoblotting detection of ABCB1 WT and variants expressed in plasma membranes. (A) Protein levels of ABCB1 WT and variants expressed in plasma membranes prepared from Sf9 cells. ABCB1 was detected by immunoblotting as described in Experimental Procedures. Proteins in Sf9 plasma membranes (2.5  $\mu$ g each) were separated by 7.5% SDS-PAGE. ABCB1 WT and variants were detected by specific monoclonal antibody C219 and the anti-mouse IgG-HRP conjugate. HRP-dependent chemiluminescence was detected in a Lumino Imaging Analyzer FAS-1000. The relative levels of ABCB1 WT and variant proteins in the plasma membrane were calculated from the calibration curve of the ABCB1 protein level vs the signal intensity. Data are expressed as mean values  $\pm$  SD ( $n = 3$ ). (B) Relationship between the ABCB1 protein level and the intensity of chemiluminescence. Plasma membranes (0, 0.25, 0.5, 1.0, 2.0, and 5.0  $\mu$ g of protein) of Sf9/ABCB1 WT cells were analyzed by immunoblotting. The signal intensity of ABCB1 was plotted as a function of the logarithmic value of membrane protein. Signal intensity =  $19.8 \log [\text{membrane protein}] + 1.59$  ( $R^2 = 0.983$ ). (C) Effect of vanadate on the basal and drug-stimulated ATPase activities. Sf9 plasma membranes (2  $\mu$ g of protein) expressing ABCB1 WT and variants (A893P, A893S, and A893T) were incubated with ATP (2 mM) and verapamil (20  $\mu$ M) in the presence of sodium *o*-vanadate (vanadate) at different concentrations (0, 10, 20, 50, and 100  $\mu$ M) at 37  $^{\circ}$ C for 30 min. After the incubation, the amount of liberated phosphate was measured as described in Experimental Procedures. Data are expressed as mean values  $\pm$  SD ( $n = 3$ ). (D) Correlation between the drug-stimulated ATPase activity and the amount of ABCB1 protein in Sf9 plasma membrane preparations. The relative amounts of ABCB1 protein in membrane preparations were measured by immunoblotting and quantified, as described above. Sf9 plasma membrane preparations (a total of 2  $\mu$ g of membrane protein) expressing ABCB1 WT and variants (A893P, A893S, and A893T) were incubated with ATP (2 mM) and verapamil (20  $\mu$ M) at 37  $^{\circ}$ C for 30 min. The verapamil-stimulated ATPase activity was determined.

heated from 0 to 310 K ( $-273$  to  $37$   $^{\circ}$ C) in 400 ps and equilibrated at 310 K (37  $^{\circ}$ C) for 100 ps. The time step of the simulations was 2 fs. Temperature was controlled at 310 K (37  $^{\circ}$ C) by Berendsen's algorithm (44). The SHAKE method was applied to constrain all bonds connecting hydrogen atoms (45). To represent the effect of membrane environments, harmonic constraints with a strength of 4 kcal/(mol $\cdot$  $\text{\AA}^2$ ) were applied to all atoms in the transmembrane (TM) regions of TM10 (amino acids 858–882) and TM11 (amino acids 945–964). MD calculation was performed to simulate the movement of the intracellular loop located between TM10 and TM11 for each variant protein (A893S, A893T, or A893P) as well as the WT.

**Statistical Analysis.** Experimental data were expressed as relative values  $\pm$  SD of more than three experiments. All statistical analyses were performed by using Microsoft Excel 2003 software (Microsoft Co., Redmond, WA). The statistical significance of differences between WT and each variant type was determined according to the two-sided Student's *t*-test. *p* values  $<0.05$  or  $<0.01$  were considered statistically significant.

## RESULTS

**Expression of SNP Variants of ABCB1 in Insect Cells.** On the basis of the ABCB1 (WT) cDNA cloned from a human liver cDNA library, those variant forms (i.e., S400N, R492C, R669C, I849M, A893P, A893S, A893T, M986V, A999T, P1051A, and G1063A) were generated by site-directed mutagenesis as described in Experimental Procedures. The variant forms as well as the WT of ABCB1 were then expressed in Sf9 cells by using the pFastBac1 vector and recombinant baculoviruses. The plasma membrane fraction was prepared from those cells. The upper panel of Figure 2A demonstrates the protein levels of those variants and the WT of ABCB1 detected by immunoblotting, where differences in ABCB1 protein levels among the plasma membrane preparations were observed in the signal intensity of immunoblotting. To quantitatively analyze the activity of ABCB1 variants, it is critically important to normalize the expression level of each variant protein. The C219 monoclonal antibody reportedly recognizes the epitopes corresponding to amino acids 568–581 (VVQEALDKARKGRT) and 1213–1226 (VVQEALDKAREGRT) of ABCB1 (46), and all of the variants expressed in Sf9 cells had the same epitope

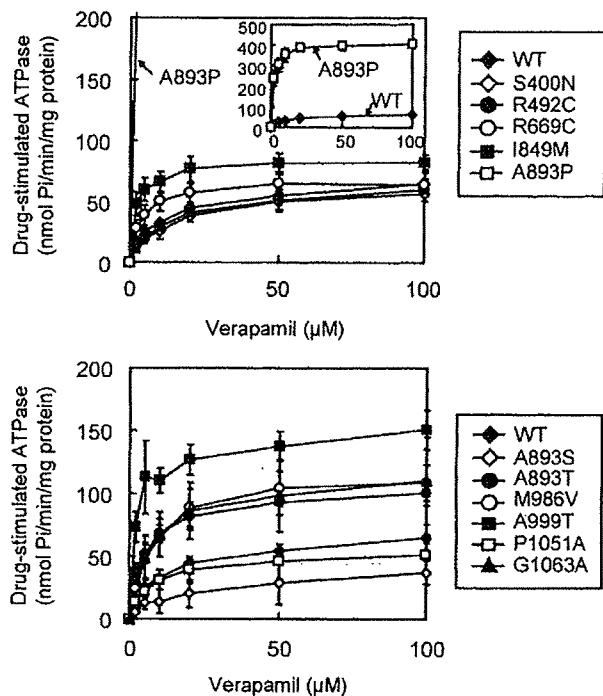


FIGURE 3: Verapamil-stimulated ATPase activity of ABCB1 WT and SNP variants. Sf9 plasma membranes (2  $\mu$ g of protein) expressing ABCB1 WT and variants (S400N, R492C, R669C, I849M, A893P, A893S, A893T, M986V, A999T, P1051A, and G1063A) were incubated with ATP (2 mM) and verapamil at different concentrations (0, 1, 2, 5, 10, 20, 50, and 100  $\mu$ M) at 37  $^{\circ}$ C for 30 min. After the incubation, the amount of liberated phosphate was measured as described in Experimental Procedures. All activities are expressed as mean values  $\pm$  SD ( $n = 6$ ).

Table 2:  $K_m$  and  $V_{max}$  Values for ATPase Activity of ABCB1 WT and Variants toward Verapamil<sup>a</sup>

SNP	$K_m$ ( $\mu$ M)	$V_{max}$ [nmol min <sup>-1</sup> (mg of protein) <sup>-1</sup> ]	$V_{max}/K_m$
WT	5.8 $\pm$ 2.3	62.4 $\pm$ 7.8	10.8
S400N	5.8 $\pm$ 2.8	46.7 $\pm$ 5.3**	8.0
R492C	5.6 $\pm$ 1.9	49.6 $\pm$ 10.0*	8.9
R669C	3.2 $\pm$ 1.6*	64.7 $\pm$ 6.9	20.1
I849M	1.5 $\pm$ 0.7**	80.3 $\pm$ 9.5**	51.8
A893P	1.5 $\pm$ 0.5**	405.2 $\pm$ 16.5**	274.6
A893S	11.1 $\pm$ 5.4	43.1 $\pm$ 7.1**	3.9
A893T	4.3 $\pm$ 1.4	98.9 $\pm$ 9.5**	22.9
M986V	5.1 $\pm$ 1.1	114.9 $\pm$ 13.6**	22.5
A999T	2.0 $\pm$ 0.8**	143.1 $\pm$ 21.2**	70.9
P1051A	6.2 $\pm$ 3.0	52.1 $\pm$ 13.6	8.4
G1063A	6.2 $\pm$ 3.7	117.9 $\pm$ 16.4**	19.0

<sup>a</sup>Data are expressed as mean  $\pm$  SD,  $n = 6$ . \* $p < 0.05$ ; \*\* $p < 0.01$ .

sequences. Figure 2B clearly demonstrates a linear relationship between the signal intensity of immunoblotting and the logarithmic value of the amount of protein applied to the electrophoresis. Similar relationships were observed with variants proteins, as well. On the basis of the linear relationship, the expression levels of ABCB1 WT and its variants in different plasma membrane preparations were quantitatively estimated and normalized (Figure 2A, bottom panel).

**Effect of Verapamil and Nicardipine on ATPase Activity of ABCB1 WT and Variants.** Since verapamil is reportedly a typical substrate for ABCB1, we first tested verapamil-stimulated ATPase activity in the plasma membranes pre-

Table 3:  $K_m$  and  $V_{max}$  Values for ATPase Activity of ABCB1 WT and Variants toward Nicardipine<sup>a</sup>

SNP	$K_m$ ( $\mu$ M)	$V_{max}$ [nmol min <sup>-1</sup> (mg of protein) <sup>-1</sup> ]	$V_{max}/K_m$
WT	1.1 $\pm$ 0.6	45.2 $\pm$ 8.7	41.0
S400N	1.7 $\pm$ 0.8	39.1 $\pm$ 9.1	23.4
R492C	1.1 $\pm$ 0.5	46.6 $\pm$ 6.4	43.5
R669C	0.3 $\pm$ 0.3**	53.5 $\pm$ 13.1	164.6
I849M	0.8 $\pm$ 0.9	80.2 $\pm$ 9.6**	102.9
A893P	0.1 $\pm$ 0.0**	341.2 $\pm$ 36.6**	4858.4
A893S	2.0 $\pm$ 0.6	39.2 $\pm$ 6.0	19.5
A893T	0.4 $\pm$ 0.2**	77.0 $\pm$ 16.9**	207.8
M986V	0.7 $\pm$ 0.4	89.7 $\pm$ 17.7**	129.9
A999T	0.3 $\pm$ 0.3**	115.4 $\pm$ 21.2**	393.6
P1051A	0.9 $\pm$ 0.3	33.1 $\pm$ 8.8*	36.3
G1063A	0.8 $\pm$ 0.4	93.2 $\pm$ 27.6**	121.4

<sup>a</sup>Data are expressed as mean  $\pm$  SD,  $n = 6$ . \* $p < 0.05$ ; \*\* $p < 0.01$ .

pared from Sf9 cells expressing ABCB1 WT. Such verapamil-stimulated activity was not detected in the plasma membranes prepared from the control cells infected with mock virus (refer to Figure 10 in ref 32). Membrane preparations from both control and ABCB1-expressing Sf9 cells exhibited basal ATPase activities that were little affected by *o*-vanadate at concentrations up to 100  $\mu$ M (Figure 2C) but inhibited by 1 mM beryllium chloride, a nonspecific ATPase inhibitor (data not shown). On the other hand, the verapamil-stimulated ATPase activity was vanadate-sensitive. As shown in Figure 2C, the drug-stimulated ATPase activities of ABCB1 WT and the A893S, A893T, and A893P variants were completely inhibited by 20  $\mu$ M *o*-vanadate. Furthermore, linear correlations were observed between the verapamil-stimulated vanadate-sensitive ATPase activity and the amounts of the ABCB1 protein in Sf9 plasma membranes expressing WT or SNP variants (Figure 2D). Therefore, it is concluded that the drug-stimulated ATPase activity reflects the function of ABCB1 and that the activity could be normalized by considering the ABCB1 protein levels determined by immunoblotting. In this context, we measured the drug-stimulated ATPase activity throughout this study.

To characterize the effect of nonsynonymous polymorphisms on the ABCB1 function, we measured the verapamil-stimulated ATPase activity by incubating the membrane preparation with verapamil at different concentrations (0–100  $\mu$ M) for each variant and the WT. Figure 3 depicts the verapamil-stimulated ATPase activity of ABCB1 WT, S400N, R492C, R669C, I849M, A893P, A893S, A893T, M986V, A999T, P1051A, and G1063A, where the verapamil-stimulated ATPase activities are normalized by considering the ABCB1 protein amounts.

As demonstrated in Figure 3, the verapamil-stimulated ATPase activity varied among those variants. For all of the variants tested, saturation kinetics was observed in the relationship between the verapamil-stimulated ATPase activity and the verapamil concentration, suggesting Michaelis–Menten kinetics. Thus,  $K_m$  and  $V_{max}$  values were calculated from Lineweaver–Burk plots of (verapamil-stimulated ATPase activity)<sup>-1</sup> vs (verapamil concentration)<sup>-1</sup> for each variant and WT (data not shown). A893P, I849M, A893T, M986V, and G1063A variants showed higher  $V_{max}$  values than did the WT, whereas the  $V_{max}$  value of A893S was lower than that of WT. It is noteworthy that the A893P variant